Time of Matching Reduction and Improvement of Sub-Optimal Image Segmentation for Iris Recognition

R. M. Farouk[1], G. F. Elhadi[2]

[1] Department of Mathematics, Faculty of Science, Zagazig University, Zagazig, Egypt.

[2] Computer Science Department, Faculty of Computers and Information's, Menofia University, Menofia, Egypt.

Abstract

In this paper, a new matching scheme based on the scalar product (SP) between two templates is used in the matching process. We also introduced the active contour technique to detect the inner boundary of the iris which is not often a circle and the circular Hough transform to determine the outer boundary of the iris. The active contour technique takes into consideration that the actual pupil boundary is near-circular contour rather than a perfect circle, which localize the inner boundary of the iris perfectly. The 1-D log-Gabor filter is used to extract real valued template for the normalized iris. We apply our system on two publicly available databases (CASIA and UBIRIS) and the numerical results show that, perfectly matching process and also the matching time is reduced. We also compare our results with previous results and find out that, the matching with SP is faster than the matching with other techniques.

Keywords: Biometric, Iris Recognition, Segmentation, Active Contour, Normalization, Feature Extraction, Matching, Scalar Product.

1. Introduction

The developments in science and technology have made it possible to use biometrics in applications where it is required to establish or confirm the identity of individuals. Applications such as passenger control in airports, access control in restricted areas, border control, database access and financial services are some of the examples where the biometric technology has been applied for more reliable identification and verification.
Biometrics is inherently a more reliable and capable technique to identity human's authentication by his or her own physiological or behavioral characteristics. The features used for personnel identification by current biometric applications include facial features, fingerprints, iris, palm-prints, retina, handwriting signature, DNA, gait, etc [17, 23]. The human iris is an annular part between pupil and sclera and its complex pattern contains many distinctive features such as arching ligaments, furrows, ridges, crypts, corona, and freckles Figure. 1. At the same time the iris is protected from the external environment behind the cornea and the eyelids. No subject to deleterious effects of aging, the small-scale radial features of the iris remain stable and fixed from about one year of age throughout one's life. The reader's two eyes, directed at this page, have identical genetics; they will likely have the same color and may well show some large scale pattern similarities; nevertheless, they have quite different iris pattern details.

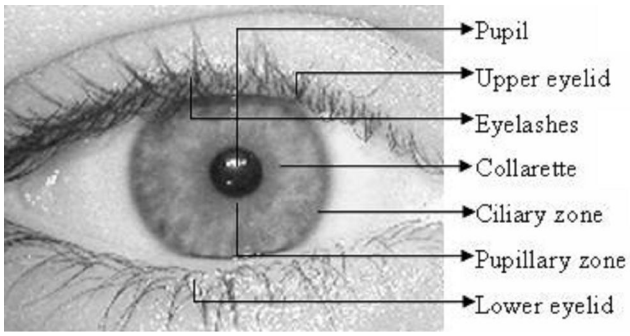

Fig 1: The image (Img 141 1 1) from the UBIRIS database

All these advantages let the iris recognition be a promising topic of biometrics and get more and more attention [7, 8, 26]. Even though iris is seen as the most reliable biometric measure, it is still not in everyday use because of the complexity of the systems. In an iris recognition system, iris location is an essential step that spends nearly more than half of the entire processing time [36]. The correctness of iris location is required for the

latter processes such as normalization, feature extraction and pattern matching. For those reasons, to improve the speed and accuracy of iris location becomes nontrivial. The algorithm proposed in this work is improvement of the matching process in the algorithms proposed by Daugman [8, 9]. The United Arab Emirates Expellees Tracking and Border Control System [22] is an outstanding example of the technology.

In general, the process of iris recognition system consists of: (i) image acquisition, (ii) Preprocessing the iris image including iris localization, image normalization and polar transformation, (iii) iris Feature extraction and (iv) iris matching.

1.1 Related Work

The research in the area of iris recognition has been receiving considerable attention and a number of techniques and algorithms have been proposed over the last few years. Flom and Safir first proposed the concept of automated iris recognition in [18]. The approach presented by Wildes [26] combines the method of edge detection with Hough transform for iris location. However, the parameters need to be precisely set and lengthy location time is required. Daugman's method is developed first using the integro-differential operator [10] for localizing iris regions along with removing possible eyelid noises. In the past few years, some methods made certain improvement based on the Daugman's method [8, 9]. Bowyer et al. [17] recently presented an excellent review of these methods. However, at this time, essentially all of the large scale implementations of iris recognition are based on the Daugman iris recognition algorithms [8]. The difference between a pair of iris codes was measured by their Hamming distance. Sanchez-Reillo and Sanchez-Avila [27] provided a partial implementation of the algorithm by Daugman. Boles and Boashash [34] calculated a zero-crossing representation of one-dimensional wavelet transform at various resolution levels of a concentric circle on an iris image to characterize the texture of the iris. Iris matching was based on two dissimilarity functions. [29] Decomposed an iris image into four levels using 2-D Haar wavelet transform and quantized the fourth-level high-frequency information to form an 87-bit code. A modified competitive learning neural network was adopted for classification. Tisse et al. [5] analyzed the iris characteristics using the analytic image constructed by the original image and its Hilbert transform. Emergent frequency functions for feature extraction were in essence samples of the phase gradient fields of the analytic image's dominant components [17, 31].

Similar to the matching scheme of Daugman, they sampled binary emergent frequency functions to form a feature vector and used Hamming distance for matching. Kumar et
al. [3] utilized correlation filters to measure the consistency of iris images from the same eye. The correlation filter of each class was designed using the two-dimensional Fourier transforms of training images. If the correlation output (the inverse Fourier transform of the product of the input images Fourier transform and the correlation filter) exhibited a sharp peak, the input image was determined to be from an authorized subject, otherwise an impostor one. Bae et al. [16] projected the iris signals onto a bank of basis vectors derived by independent component analysis and quantized the resulting projection coefficients as features. In another approach by Ma et al. [19] and Even Symmetry Gabor filters [10] are used to capture local texture information of the iris, which are used to construct a fixed length feature vector.

In the last year only, the iris takes the attention of many researchers and different ideas are formulated and published. For example, in [1] a bi-orthogonal wavelet based iris recognition system, is modified and demonstrated to perform o_-angle iris recognition. An efficient and robust segmentation of noisy iris images for non-cooperative iris recognition is described in [32]. Iris image segmentation and sub-optimal images is discussed in
[13]. Comparison and combination of iris matchers for reliable personal authentication are introduced in [2]. Noisy iris segmentation, with boundary regularization and reflections removal, is discussed in [28].

1.2 Outline

In this paper, we first present the active contour models for iris preprocessing (segmentation step) which is a crucial step to the success of any iris recognition system, since data that is falsely represented as iris pattern data will corrupt the biometric templates generated, thus resulting in poor recognition rates. Once the iris region is successfully segmented from an eye image, the next stage is to transform the iris region so that it has fixed dimensions (normalization) in order to allow comparisons using Daugman rubber sheet model. After that the 1-D log-Gabor filter is used to extract real valued template for the normalized iris.

2. Iris Localization Techniques

It is the stage of locating the iris region in an eye image, whereas mentioned the iris region is the annular part

between pupil and sclera, see Figure 1. The iris segmentation has achieved by the following three main steps. The first step locates the center and radius of the iris in the input image by using the circular hough transform. Then a set of points is taken as pupil initialization from the nearby points to the iris center. The last step locates the pupil boundary points by using the region-based active contours.

2.1 Hough Transform

The Hough transform is a standard computer vision algorithm that can be used to determine the parameters of simple geometric objects, such as lines and circles, present in an image. The circular Hough transform can be employed to deduce the radius and center coordinates of the pupil and iris regions. For instance, recognition of a circle can be achieved by considering the strong edges in an image as the local patterns and searching for the maximum value of the circular Hough transform. An automatic segmentation algorithm based on the circular Hough transform is employed by Wildes et al. [26], and Tisse et al. [5].

The localization method, similar to Daugman's method, is also based on the first derivative of the image. In the proposed method by Wildes, an edge map of the image is first obtained by thresholding the magnitude of the image intensity gradient:

$$\left|\nabla G(x,y) * I(x,y)\right|, \quad (1)$$

$$G(x,y) = \frac{1}{2\pi\sigma^2}\exp -\left(\frac{(x-x_0)^2+(y-y_0)^2}{2\sigma^2}\right) \quad (2)$$

Where $G(x,y)$ is a Gaussian smoothing function with scaling parameter σ to select the proper scale of edge analysis. Firstly, an edge map is generated by calculating the first derivatives of intensity values in an eye image and then thresholding the result. From the edge map, votes are cast in Hough space to maximize the defined Hough transform for the desired contour. Considering the obtained edge points as for the parameters of circles passing through each edge points as $(x_i, y_i), i = 1,2,3,.....n$. These parameters are the center coordinates x_c and y_c, and the radius r, which are able to define any circle according to the equation:

$$x_c^2 + y_c^2 = r^2 \quad (3)$$

A Hough transform can be written as:

$$H(x_c, y_c, r) = \sum_{1}^{n} h(x_i, y_i, x_c, y_c, r) \quad (4)$$

$$h(x_i, y_i, x_c, y_c, r) = \begin{cases} 1 & if\ g(x_i, y_i, x_c, y_c, r) = 0 \\ 0 & otherwise \end{cases} \quad (5)$$

Where the parametric function

$g(x_i,y_i,x_c,y_c,r)=(x_i-x_c)^2+(y_i-y_c)^2-r^2$.

Assuming a circle with the center (x_c, y_c) and radius r, the edge points that are located over the circle result in a zero value of the function g. The value of g is then transformed to 1 by the h function, which represents the local pattern of the contour. The local patterns are then used in a voting procedure using the Hough transform, H, in order to locate the proper pupil and limbus boundaries. In order to detect limbus, only vertical edge information is used. The upper and lower parts, which have the horizontal edge information, are usually covered by the two eyelids. The horizontal edge information is used for detecting the upper
and lower eyelids, which are modeled as parabolic arcs.

2.2 Active Contour Models

Ritter et al. [24] make use of active contour models for localizing the pupil in eye images. Active contours respond to pre-set internal and external forces by deforming internally or moving across an image until equilibrium is reached. The contour contains a number of vertices, whose positions are changed by two opposing forces, an internal force, which is

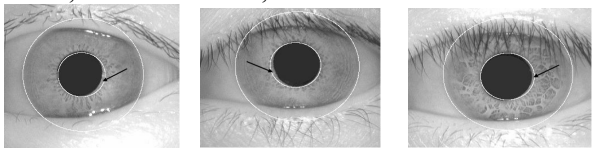

(a) (b) (c)

Figure 2: Errors in pupil localization by using the circular Hough transform.

dependent on the desired characteristics, and an external force, which is dependent on the image. Each vertex is moved between time t and $t + 1$ by:

$$V_i(t+1) = V_i(t) + F_{\text{int},i}(t) + F_{ext,i}(t) \quad (6)$$

Where $F_{int,i}$ is the internal force, $F_{ext,i}$ is the external force and Vi is the position of vertex i. For localization of the pupil region, the internal forces are calibrated so that the contour forms a globally expanding discrete circle. The external forces are usually found using the edge information.

In order to improve accuracy Ritter et al. use the variance image, rather than the edge image. A point interior to the pupil is located from a variance image and then a discrete circular active contour (DCAC) is created with this point as its center. The DCAC is then moved under the influence of internal and external forces until it reaches equilibrium, and the pupil is localized.

2.3 Discrete Circular Active Contour

Ritter (2003) et al. [25] proposed a model which detects pupil and limbus by activating and controlling the active contour using two defined forces: internal and external forces.

The internal forces are responsible to expand the contour into a perfect polygon with a radius σ larger than the contour average radius. The internal force $F_{int,i}$ applied to each vertex, *Vi*, is defined as

$$F_{\text{int},i} = \overline{V_i} - V_i \quad (7)$$

where $\overline{V_i}$ is the expected position of the vertex in the perfect polygon. The position of $\overline{V_i}$ can be obtained with respect to C_r, the average radius of the current contour, and the contour center, $C = (C_x; C_y)$. The center of a contour which is the average position of all contour vertices is defined as

$$C = (C_x, C_y) = \frac{1}{n}\sum_{i=1}^{n} V_i \quad (8)$$

The average radius of the contour is the average distance of all the vertices from the defined center point C is as the following equations

$$C_r = \frac{1}{n}\sum_{i=1}^{n} \|V_i - C\| \quad (9)$$

Then the position of the vertices of the expected perfect polygon is obtained as

$$\overline{V_i} = (C_x + (C_r + \delta)\cos(2\pi i / n), \; C_y + (C_r + \delta)\cos(2\pi i / n)) \quad (10)$$

where *n* is the total number of vertices.

The internal forces are designed to expand the contour and keep it circular. The force model assumes that pupil and limbus are globally circular, rather than locally, to minimize the undesired deformations due to specular reflections and dark patches near the pupil boundary. The contour detection process of the model is based on the equilibrium of the defined internal forces with the external forces. The external forces are obtained from the grey level intensity values of the image and are designed to push the vertices inward. The magnitude of the external forces is defined as:

$$\|F_{ext,i}\| = I(V_i) - I(V_i + \hat{F}_{ext,i}) \quad (11)$$

where $I(V_i)$ is the grey level value of the nearest neighbor to V_i. $\hat{F}_{ext,i}$ is the direction of the external force for each vertex and it is defined as a unit vector given by:

$$\hat{F}_{ext,i} = \frac{C - V_i}{\|C - V_i\|} \quad (12)$$

Therefore, the external force over each vertex can be written as:

$$F_{ext,i} = \|F_{ext,i}\| \hat{F}_{ext,i} \quad (13)$$

The movement of the contour is based on the composition of the internal and external forces over the contour vertices. Replacement of each vertex is obtained iteratively by:

$$V_i(t+1) = V_i(t) + \beta F_{\text{int},i}(t) + (1-\beta) F_{ext,i}(t) \quad (14)$$

Where β is a defined weight that controls the pace of the contour movement and sets the equilibrium condition of internal and external forces. The final equilibrium is achieved when the average radius and center of the contour becomes the same for the first time in *m* iterations ago. The discrete circular active contour is applied on the three images in Figure 3.

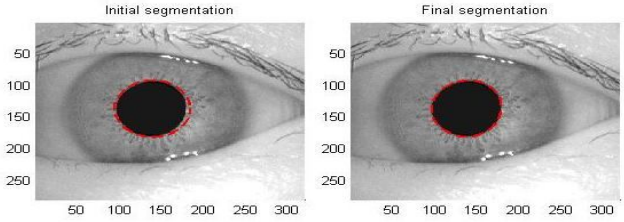

Figure 3: The segmentation of the DCA

2.4 Detecting Eyelids, Eyelashes and Noise Regions

The eyelids are detected by first fitting a line to the upper and lower eyelid using the linear Hough transform. A horizontal line is then drawn which intersects with the first line at the iris edge that is closest to the pupil. A second horizontal line allows the maximum isolation of eyelid regions.

Detecting eyelashes requires proper choice of features and classification procedure due to complexity and randomness of the patterns. The proposed eyelash detection by Kong et

al. consider eyelashes as two groups of separable eyelashes, which are isolated in the image, and multiple eyelashes, which are bunched together and overlap in the eye and applies two different feature extraction methods to detect eyelashes [35]. Separable eyelashes are detected

using 1-D Gabor filter, since the convolution of a separable eyelash with the Gaussian smoothing function results in a low output value.
Thus, if a resultant point is smaller than a threshold, it is noted that this point belongs to an eyelash. Multiple eyelashes are detected using the variance of intensity. If the
variance of intensity values in a small window is lower than a threshold, the center of the window is considered as a point in an eyelash. The two features combined with a
connectivity criterion would lead to the decision of presence of eyelashes. In addition, an eyelash detection method is also proposed by Huang et al. that uses the edge information obtained by phase congruency of a bank of Log-Gabor filters. The edge information is also infused with the region information to localize the noise regions [15], as in Figure 4.

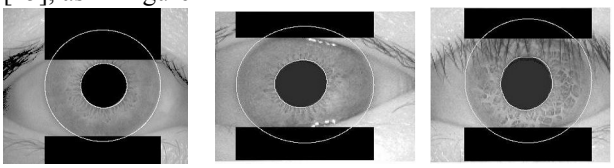

Figure 4: illustrates the perfect iris localization, where black regions denote detected eyelids and eyelashes regions.

3. Normalization

Once the iris region is successfully segmented from an eye image, the next stage is to transform the iris region so that it has fixed dimensions in order to eliminate dimensional inconsistencies between iris regions, and to allow comparisons. The dimensional inconsistencies between eye images are mainly due to the stretching of the iris caused by pupil dilation from varying levels of illumination. Other sources of inconsistency include, varying imaging distance, rotation of the camera, head tilt, and rotation of the eye within the eye socket. The normalization process will produce iris regions, which have the same constant dimensions, so that two images of the same iris under different conditions will have the same characteristic features at the same spatial location. A proper normalization technique is expected to transform the iris image to compensate these variations.
Most normalization techniques are based on transforming iris into polar coordinates, known as unwrapping process. Pupil boundary and limbus boundary are generally two non-concentric contours. The non-concentric condition leads to different choices of reference points for transforming an iris into polar coordinates. Proper choice of reference point is very important where the radial and angular information would be defined with respect to this point. Unwrapping iris using pupil center is proposed by Boles and Boashash [34] and Lim et al. [14]. Another reference point proposed by Arvacheh [6], which is the virtual center of a pupil with radius equal to zero (linearly-guessed center). The experiments demonstrate that the linearly-guessed center provides much better recognition accuracy. The linearly-guessed center is equivalent to the technique used by Joung et al. [4].
In addition, most normalization approaches based on Cartesian to polar transformation unwrap the iris texture into a fixed-size rectangular block. For example, in Lim et al. method, after finding the center of pupil and the inner and outer boundaries of iris, the texture is transformed into polar coordinates with a fixed resolution. In the radial direction, the texture is normalized from the inner boundary to the outer boundary into 60 pixels. The angular resolution is also fixed to a 0:8o over the 360o, which produces 450 pixels in the angular direction. Other researchers such as Boles and Boashash, Tisse et al. [5]. And Ma et al. [20] also use the fixed size polar transformation model.
However, the circular shape of an iris implies that there are different number of pixels over each radius. Transforming information of different radii into same resolution results in different amount of interpolations, and sometimes loss of information, which may degrade the performance of the system.

3.1 Daugman's Rubber Sheet Model

It transforms a localized iris texture from Cartesian to polar coordinates. It is capable of compensating the unwanted variations due to distance of eye from camera (scale) and its position with respect to the camera (translation). The Cartesian to polar transformation is defined as

$$I((x(r,\theta), y(r,\theta)) \rightarrow I(r,\theta) \quad (15)$$

where

$$x(r,\theta) = (1-r)\times x_p(\theta) + r \times x_i(\theta),$$
$$y(r,\theta) = (1-r)\times y_p(\theta) + r \times y_i(\theta),$$

and

$$x_p(\theta) = x_{p0}(\theta) + r_p \times \cos(\theta),$$
$$y_p(\theta) = y_{p0}(\theta) + r_p \times sn(\theta),$$
$$x_i(\theta) = x_{i0}(\theta) + r_i \times \cos(\theta),$$
$$y_i(\theta) = y_{i0}(\theta) + r_i \times \sin(\theta),$$

where $I(x; y)$ is the iris region image, $(x; y)$ are the original Cartesian coordinates, (r,θ) are the corresponding normalized polar coordinates, and $(x_p; y_p)$ and $(x_i; y_i)$ are the coordinates of the pupil and iris boundaries along the _ direction. The process is inherently dimensionless in the angular direction. In the radial direction, the texture is

assumed to change linearly, which is known as the rubber sheet model, as shown in Figure 5.

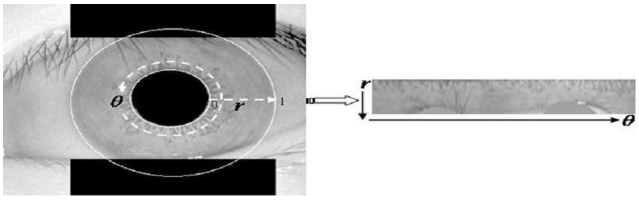

Figure 5: The rubber sheet model for normalizing the segmented irises.

The rubber sheet model [30] linearly maps the iris texture in the radial direction from pupil border to limbus border into the interval [0 1] and creates a dimensionless transformation in the radial direction as well. It takes into account pupil dilation and size inconsistencies in order to produce a normalized representation of constant dimensions. In this way the iris region is modeled as a flexible rubber sheet anchored at the iris boundary with the pupil center as the reference point.

Although the normalization method compensates variations due to scale, translation and pupil dilation, it is not inherently invariant to the rotation of iris. Rotation of an iris in the Cartesian coordinates is equivalent to a shift in the polar coordinates. In order to compensate the rotation of iris textures, a best of n test of agreement technique is proposed by Daugman in the matching process. In this method, iris templates are shifted and compared in n different directions to compensate the rotational effects. The rubber sheet model is applied on 4 different iris images, as shown in Figure 6.

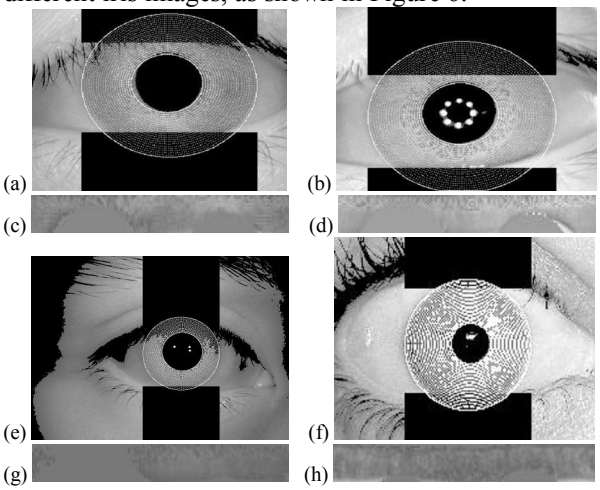

Figure 6: The normalized iris image and its polar form to four different iris images by using rubber sheet model, where (a) is an image from the CASIA-Iris V. 1, (b) is an image from the CASIA-Iris V. 3-Interval, (e) is an image from the CASIA-Iris V. 3-Lamp, and (f) is an image from the UBIRIS database. (c), (d), (g) and (h) are the polar form to the four iris images respectively.

4. Feature extraction

In order to provide accurate recognition of individuals, the most discriminating information present in an iris pattern must be extracted. Only the significant features of the iris must be encoded so that comparisons between templates can be made. Most iris recognition systems make use of a band pass decomposition of the iris image to create a biometric template.

The first step after the iris normalization is to extract the features from the normalized iris image. The Gabor wavelet method with log-polar transformation was designed by Daugman in 1993 and is widely used in commercialized iris recognition systems [10]. The log-Gabor wavelet method with Polar transformation was designed by Masek and Kovesi and implemented in Matlab

[21]. Wavelets can be used to decompose the data in the iris region into components that appear at different resolutions. Wavelets have the advantage over traditional Fourier transform in that the frequency data is localized, allowing features which occur at the same position and resolution to be matched up. A number of wavelet filters, also called a bank of wavelets, are applied to the 2-D iris region, one for each resolution with each wavelet a scaled version of some basis function. The output of applying the wavelets is then encoded in order to provide a compact and discriminating representation of the iris pattern.

Some works have used multi-resolution techniques for iris feature extraction [8, 26, 34] and have proven a high recognition accuracy. At the same time, however, it has been observed that each multi-resolution technique has its specification and situation in which it is suitable; for example, a Gabor filter bank has been shown to be most known multi-resolution method used for iris feature extraction and Daugman [8] in his proposed iris recognition system demonstrated the highest accuracy by using Gabor filters.

4.1 The 1-D Log-Gabor Filter

The 1-D log-Gabor band pass filter is used to extract the features in an iris [35, 36], it is defined as

$$G(w) = \exp\left(\frac{-\log(w/w_0)^2}{2\log(\sigma^2)}\right) \quad (16)$$

where, σ is used to control the filter bandwidth and ! is the filter's center frequency, which is derived from the filter's wavelength, λ. The 1-D log-Gabor filter does not have a spatial domain format. Each row of the iris image, in the log-polar coordinates, is first transformed to the frequency domain using fast Fourier transform (FFT). This frequency domain row signal is then filtered with the

1-D log-Gabor filter (i.e. multiplied with the 1-D log-Gabor filter in the frequency domain).
The filtered row signal is transferred back to the spatial domain via inverse fast Fourier transform (IFFT). The spatial domain signal is then transferred to a filtered image in the spatial domain, and hence the biometric code (template) is obtained from the filtered image.
Figure 7 shows the step-by-step process of the 1-D log Gabor filter feature extraction.

5. Matching

Once an iris image relevant texture information extracted, the resulting feature vector (iris template) is compared with enrolled iris templates. The template generated needs a corresponding matching metric, which gives a measure of similarity between two iris templates. This metric should give one range of values when comparing templates generated from the same eye, known as intra-class comparisons, and another range of values when comparing templates created from different irises, known as extra-class comparisons.
These two cases should give distinct and separate values, so that a decision can be made with high confidence as to whether two templates are from the same iris, or from two different irises. The following subsections introduce some famous matching metrics, and finally the scalar product (SP) method.

5.1 The Normalized Hamming Distance

The Hamming distance (HD) gives a measure of how many bits are the same between two bit patterns, especially if the template is composed of binary values. Using the HD of two bit patterns, a decision can be made as to whether the two patterns were generated from different irises or from the same iris. For example, comparing the bit patterns P and Q, the HD is defined as the sum of disagreeing bits (sum of the exclusive-OR between P and Q) over N, the total number of bits in each bit pattern. It is known as the normalized HD, and is defined as:

$$HD = \frac{1}{N}\sum_{i=1}^{N} P_i \otimes Q_i \quad (17)$$

Since an individual iris region contains features with high degrees of freedom, each iris region will produce a bit-pattern which is independent to that produced by another iris, on the other hand, two iris codes produced from the same iris will be highly correlated.
In case of two completely independent bit patterns, such as iris templates generated from different irises, the HD between the two patterns should equal 0.5. This occurs because independence implies that, the two bit patterns will be totally random, so there is 0.5 chance of setting any bit to 1, and also to zero. Therefore, half of the bits will agree and half will disagree between the two patterns. If two patterns are derived from the same iris, the HD between them will be close to 0.0, since they are highly correlated and the bits should agree between the two iris codes.
Daugman [8] uses this matching metric as following, the simple Boolean Exclusive-OR operator (XOR) applied to the 2048 bit phase vectors that encode any two iris patterns, masked (AND'ed) by both of their corresponding mask bit vectors to prevent noniris artifacts from influencing iris comparisons. The XOR operator $\otimes$ detects disagreement between any corresponding pair of bits, while the AND operator $\cap$ ensures that the compared bits are both deemed to have been uncorrupted by eyelashes, eyelids, specular reflections, or other noise. The norms $\| \ \|$ of the resultant bit vector and of the AND'ed mask vectors are then measured in order to compute the fractional HD (Equation 5.18), as the mea-sure of dissimilarity between any two irises, whose two phase code bit vectors are denoted *codeP*; *codeQ* and whose mask bit vectors are denoted *maskP; maskQ*:

$$HD = \frac{\|(codeP \otimes coodeQ) \cap maskP \cap maskQ\|}{\|maskP \cap maskQ\|} \quad (18)$$

The denominator tallies the total number of phase bits that mattered in iris comparisons after artifacts such as eyelashes, eyelids, and specular reflections were discounted, so the resulting HD is a fractional measure of dissimilarity; 0.0 would represent a perfect match.

5.2 The Weighted Euclidean Distance

The weighted Euclidean distance (WED) can be used to compare two templates, especially if the template is composed of integer values. It gives a measure of how similar a collection of values are between two templates. This metric is employed by Zhu et al. [37] and is defined as:

$$WED(P) = \sum_{i=1}^{N} \frac{(f_i - f_i^{\,p})^2}{(\delta_i^{\,P})^2} \quad (19)$$

where f_i is the i^{th} feature of the unknown iris, and $f_i^{\,p}$ is the i^{th} feature of iris template *k*, and $\delta_i^{\,p}$ i is the standard deviation of the i^{th} feature in iris template *k*. The unknown iris template is found to match iris template *k*, when the WED is a minimum at *k*.

5.3 The Normalized Correlation

Wildes et al. [26] make use of Normalized correlation (NC) between the acquired and database representation for goodness of match. This is represented as:

$$NC = \frac{\sum_{i=1}^{m}\sum_{j=1}^{n}(p_1[i,j]-\mu_1)(p_2[i,j]-\mu_2)}{m*n*\sigma_1*\sigma_2} \quad (20)$$

where p_1 and p_2 are two images of size $m \times n$, μ_1 and σ_1 are the mean and standard deviation of p_1, and μ_2 and σ_2 are the mean and standard deviation of p_2. Normalized correlation is advantageous over standard correlation, since it is able to account for local variations in image intensity that corrupt the standard correlation calculation.

5.4 The Scalar Product

The Scalar product method (SP) can be used to compare two templates, especially if the template is composed of real values. It considers the two templates as two vectors and gives the $\cos(\theta)$ between the two templates. The $\cos(\theta)$ between any two templates is between -1 and 1. If $\cos(\theta)$ is close to 1, the two templates are for the same iris, but if it was close to zero, the templates are for different irises. For example suppose that we have two templates P and Q, the scalar product is defined as:

$$P.Q = \|P\|.\|Q\|\cos(\theta) \quad (21)$$

The localization of the iris and the coordinate system desc-

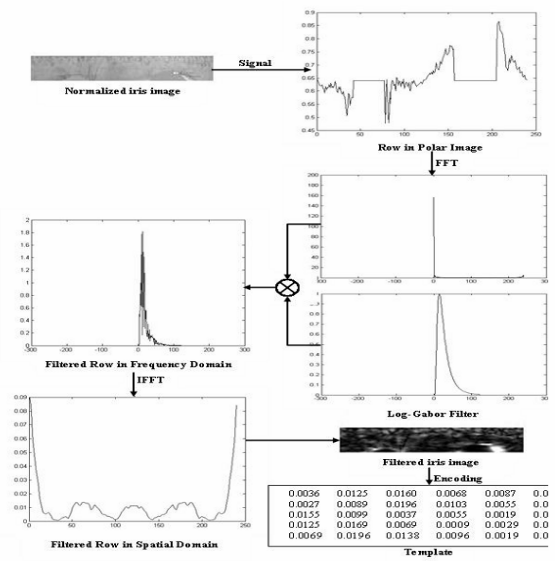

Figure 7: The step-by-step process of a row signal feature extraction by using the 1-D log-Gaber filter

Iter. No	Templates	cos(θ)
1	P = [2 6 2 1 2 8 5 10 2 3], Q = [1 2 3 4 5 6 7 8 9 10]	0:7881
2	P = [2 6 2 1 2 8 5 10 2 3], Q = [2 3 4 5 6 7 8 9 10 1]	0:8235
3	P = [2 6 2 1 2 8 5 10 2 3], Q = [3 4 5 6 7 8 9 10 1 2]	0:8911
4	P = [2 6 2 1 2 8 5 10 2 3], Q = [4 5 6 7 8 9 10 1 2 3]	0:7013
5	P= [2 6 2 1 2 8 5 10 2 3],Q= [5 6 7 8 9 10 1 2 34]	0:6723
6	P = [2 6 2 1 2 8 5 10 2 3], Q = [6 7 8 9 10 1 2 3 4 5]	0:5469
7	P = [2 6 2 1 2 8 5 10 2 3], Q = [7 8 9 10 1 2 3 4 5 6]	0:6144
8	P = [2 6 2 1 2 8 5 10 2 3], Q = [8 9 10 1 2 3 4 5 6 7]	0:7141
9	P = [2 6 2 1 2 8 5 10 2 3], Q = [9 10 1 2 3 4 5 6 7 8]	0:7817
10	P= [2 6 2 1 2 8 5 10 2 3],Q= [10 1 2 3 4 5 6 7 8 9]	0:7206

Table 1: This table indicates that, the maximum $\cos(\theta)$ = 0:8911, thus θ = 26:988 which is the smallest θ between the two templates. i.e., there is no match between the two templates for ever.

The previous table is for a simple example, but for iris the algorithm will perform 4800 iterations for comparing every two templates, because each template consists of 4800 elements.

6. Results

The actual iris image was first segmented using the gradient-based Hough transform to detect the outer iris boundary, and the DCAC for the inner iris boundary to avoid the errors of Hough transform, and then the eyelids, eyelashes, and noise regions are detected. Secondly the detected iris image is normalized using Daugman's rubber sheet model. After that the relevant texture information is extracted using the 1-D Log-Gabor filter, hence we have a real valued template of 20×240 elements which will be converted to a vector of 1×4800 elements. Finally these templates are stored to comprise a database of templates which will be used in the matching process by using the scalar product method.

This database of templates has two categories, the CASIA which consists of 996 templates and UBIRIS which consists of 723 templates. The SP method was tested by using 915 and 448iris images from CASIA and UBIRIS d-

ribed above achieve invariance to the 2-D position and size of the iris, and to the dilation of the pupil within the iris. However, it would not be invariant to the orientation of the iris within the image plane. The most efficient way to achieve iris recognition with orientation invariance is not to rotate the image itself using the Euler matrix, but rather to compute the iris phase code in a single canonical orientation and then to compare this very compact representation at many discrete orientations by cyclic scrolling of its angular variable. Thus for example to apply the SP method on two different templates P = [2 6 2 1 2 8 5 10 2 3], reference template and Q = [1 2 3 4 5 6 7 8 9

10], template from the database of 10 elements, it will work as shown in Table 1.

database respectively, and was found to give good correct recognition rates compared to other matching methods as shown in Table 2.

Matching measure	Correct recognition rate (CRR)%
WED	98.73
SP	98.26
HD	98.22

Table 2: The correct recognition rates achieved by three matching measures using the CASIA and UBIRIS database.

In our experimental results the false match rate (FMR), the rate which non-authorized people are falsely recognized during the feature comparison which contrasts the false accept rate (FAR) and the false non-match rate (FNMR), the rate that authorized people are falsely not recognized during feature comparison which contrasts the false reject rate (FRR) are estimated. Figure 8, illustrates the receiver operating characteristic (ROC) curves for the CASIA database after applying the SP matching method. Where 100-FNMR is plotted vs. the FMR.

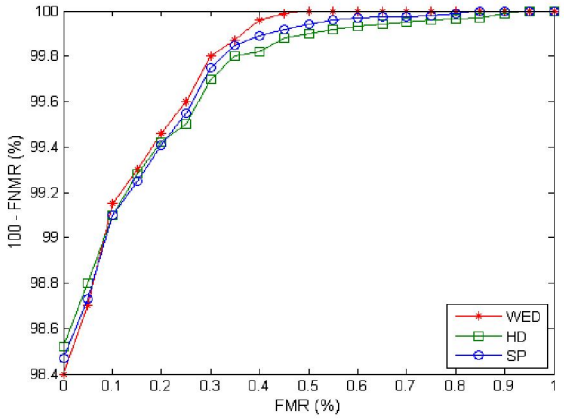

Figure 8: The obtained ROC curves to three different matching measures using the CASIA database.

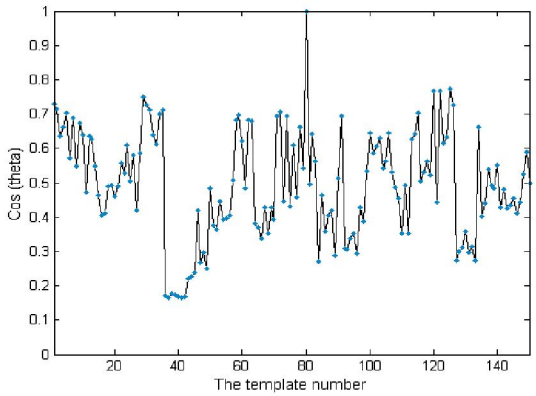

Figure 9: The matching of (012 1 3) iris image from (CASIA-Iris V. 1) with the template number 80 from 150 templates, where as shown $\cos(\theta) = 1$ between the compared iris template and the template number 80, hence the two are templates for the same iris image.

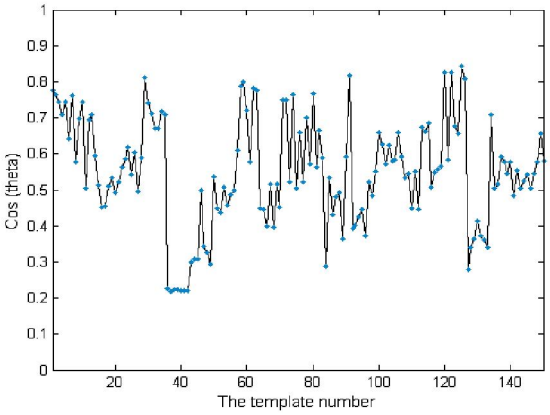

Figure 10: There is no match of (050 1 3) iris image (CASIA-Iris V. 1) with any template from 150 templates, where the maximum $\cos(\theta) = 0{:}83$ is between the compared iris template and the template number 124, hence the two templates are very similar but they are not templates for the same iris image.

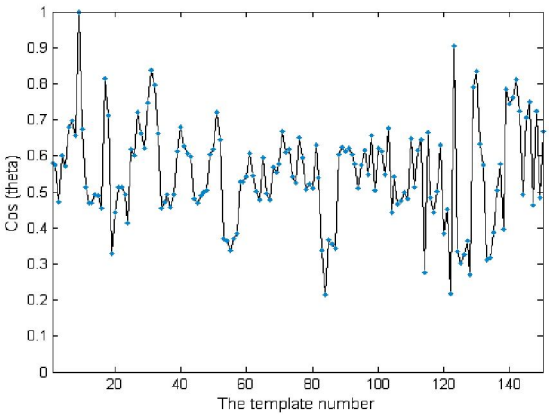

Figure 11: The matching of (Img 2 1 4) iris image from (UBIRIS database) with the template number 9 from 150 templates, where as shown $\cos(\theta) = 1$ between the compared iris template and the template number 9, hence the two are templates for the same iris image.

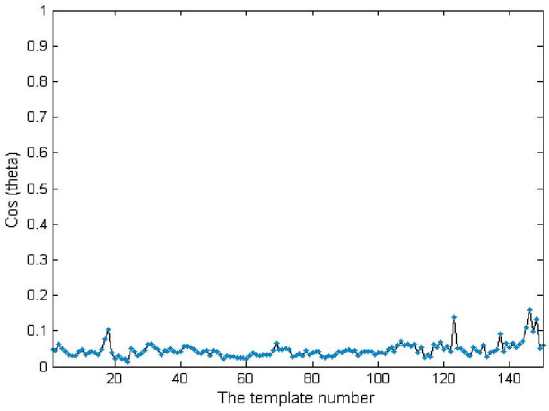

Figure 12: There is no match of (Img 235 1 5) iris image (UBIRIS database) with any template from 150 templates, where the maximum

$\cos(\theta)$ = 0:18 is between the compared iris template and the template number 145, hence the two templates are not so similar and also they are not templates for the same iris image.

7. Conclusion

Here we have presented an active contour model, in order to compensate for the iris detection error caused by two circular edge detection operations. After perfect iris localization, the segmented iris region is normalized (transformed into polar coordinates) to eliminate dimensional inconsistencies between iris regions. This was achieved by using Daugman's rubber sheet model, where the iris is modeled as a flexible rubber sheet, which is unwrapped into a rectangular block with constant polar dimensions (20×240) elements.

The next stage is to extract the features of the iris from the normalized iris region. This was done by the convolution of the 1-D Log-Gabor filters with the normalized iris region. After that the convoluted iris region is reshaped to be a template of (1_4800) real valued elements.

Finally the scalar product matching scheme is used, which give the $\cos(\theta)$ between two templates. If $\cos(\theta) = 1$ between two templates P and Q this means that, the two templates were deemed to have been generated from the same iris, otherwise they have been generated from different irises.

References

[1] A. Abhyankara, S. Schuckers, A novel biorthogonal wavelet network system for o_ angle iris recognition, Pattern Recognition, 43 (2010), 987-1007.

[2] A. Kumar, A. Passi, Comparison and combination of iris matchers for reliable personal authentication, Pattern Recognition, 43 (2010), 1016-1026.

[3] B. Kumar, C. Xie, J. Thornton, A. Bovik, Iris verification using correlation filters, Proceedings of 4th International Conference on Audio- and Video- Based Biometric Person Authentication, (2003), 697-705.

[4] B. J. Joung and C. H. Chung and K. S. Lee and W. Y. Yim and S. H. Lee, On Improvement for Normalizing Iris Region for a Ubiquitous Computing, Proceedings of International Conference on Computational Science and Its Applications ICCSA, Singapore, (2005), 1213-1219.

[5] C. Tisse, L. Martin, L. Torres, M. Robert, Person Identification Technique Using Human Iris Recognition, Proc. Vision Interface, (2002), 294-299.

[6] E. M. Arvacheh, A Study of Segmentation and Normalization for Iris Recognition Systems, University of Waterloo, Waterloo, Ontario, Canada, (2006).

[7] J. Daugman, Demodulation by Complex-valued Wavelets for Stochastic Pattern Recognition, International Journal of Wavelets, Multiresolution and Information Processing, 1 (1) (2003), 1-17.

[8] J. Daugman, How Iris Recognition Works, IEEE Transactions on Circuits and Systems for Video Technology, 14 (1) (2004), 21-30.

[9] J. Daugman, The Importance of Being Random: Statistical Principles of Iris Recognition, Pattern Recognition, 36 (2) (2003), 279-291.

[10] J.Daugman, High Confidence Visual Recognition of Persons by a Test of Statistical Independence, IEEE Transactions on Pattern Analysis and Machine Intelligence, 15 (11) (1993), 1148-1160.

[11] J. Daugman, Statistical Richness of Visual Phase Information: Update on Recognizing Persons by Iris Patterns, Int. I. J. Computer Vision, 45 (1) (2001), 25-38

[12] J. Havlicek, D. Harding, A. Bovik, The multi-component AM-FM image representation, IEEE Trans. Image Process, 5 (1996), 1094-1100.

[13] J. R. Matey, R. Broussard, L. Kennell, Iris image segmentation and sub-optimal images, Image and Vision Computing, 28 (2010), 215-222.

[14] J. Huang, Y. Wang, T. Tan, J. Cui, A new iris segmentation method for recognition, Proceedings of the 17th International Conference on Pattern Recognition, ICPR, 3 (2004), 554-557.

[15] J. Huang, Y. Wang, T. Tan, J. Cui, A new iris segmentation method for recognition, Proceedings of the 17th International Conference on Pattern Recognition, ICPR, 3 (2004), 554557.

[16] K. Bae, S. Noh, J. Kim, Iris feature extraction using independent component analysis, Proceedings of 4th International Conference on Audio- and Video-Based Biometric Person Authentication, (2003), 838-844.

[17] K. W. Boweyer, K. Hollingsworth, Patrick J. Flynn, Image understanding for iris biometrics: A survey, Computer Vision and Image Understanding, 110 (2008), 281-307.

[18] L. Flom, A. Safir, Iris recognition system, U.S. Patent, 4 (1987), 394-641.

[19] L. Ma, T. Tan, Y. Wang, D. Zhang, Efficient Iris Recognition by Characterizing Key Local Variations, IIEEE Transactions on Image Processing, 13 (2004), 739-750.

[20] L. Ma and T. Tan and Y. Wang and D. Zhang, Personal identification based on iris texture analysis, IEEE Transactions on Pattern Analysis and Machine Intelligence, 25 (12) (2003), 1519-1533.

[21] L. Masek, P. Kovesi, MATLAB Source Code for a Biometric Identification System Based on Iris Patterns, The University of Western Australia, (2003).

[22] M. Almualla, The UAE Iris Expellees Tracking and Border Control System in: Biometrics Consortium September, Crystal City, VA, (2005).

[23] N. Duta, A survey of biometric technology based on hand shape, Pattern Recognition, 42 (2009), 2797-2806.

[24] N. Ritter, Location of The Pupil-iris Border in Slit-lamp Images of The Cornea, Proceedings of the International Conference on Image Analysis and Processing, (1999).

[25] N. Ritter, J. R. Cooper, Locating the iris: A first step to registration and identification, Proceedings of the 9th

IASTED International Conference on Signal and Image Processing, (2003), 507-512.

[26] R. P. Wildes, Iris Recognition: An Emerging Biometric Technology, Proceedings of the IEEE, 85 (9) (1997), 1348-1363.

[27] R. Sanchez-Reillo, C. Sanchez-Avila, Iris recognition with low template size, Proceedings of International Conference on Audio- and Video-Based Biometric Person Authentication, (2001), 324-329.

[28] R. D. Labati, F. Scotti, Noisy iris segmentation with boundary regularization and reflections removal, Image and Vision Computing, 28 (2010), 270-277.

[29] S. Lim, K. Lee, O. Byeon, T. Kim, Efficient iris recognition through improvement of feature vector and classifier, ETRI J. 23, 2 (2001), 1-70.

[30] S. Sanderson and J. H. Erbetta, Authentication for secure environments based on iris scanning technology, IEEE Colloquium on Visual Biometrics, (2000), 1-8.

[31] T. Tangsukson, J. Havlicek, AM-FM image segmentation, Proceedings of IEEE International Conference on Image Processing, (2000), 104-107.

[32] T. Tan, Z. He, Z. Sun, Efficient and robust segmentation of noisy iris images for non-cooperative iris recognition, Image and Vision Computing, 28 (2010), 223-230.

[33] V. A. Pozdin, Y. Du, Performance analysis and parameter optimization for iris recognition using log-Gabor wavelet, SPIE Electronic Imaging 6491, (2007), 1-11.

[34] W. Boles, B. Boashash, A Human Identification Technique Using Images of The Iris and Wavelet Transform, IEEE Transactions on Signal Processing, 46 (1998), 1185-1188.

[35] W. Kong, D. Zhang, Eyelash detection model for accurate iris segmentation, Proceeding of ISCA 16th International Conference on Computers and their Applications, (2001), 204-207.

[36] X. Ye, Z. Zhuang, Y. Zhuang, A New and Fast Algorithm of Iris Location, Computer Engineering and Applications, 30 (2003), 54-56.

[37] Y. Zhu, T. Tan, Y. Wang, Biometric personal identification based on iris patterns, Proceedings of the 15 *th* International Conference on Pattern Recognition, Spain, 2 (2000).